

IMSRG-Net: A machine learning-based solver for In-Medium Similarity Renormalization Group

Sota Yoshida^{1,*}

¹*Institute for Promotion of Higher Academic Education,
Utsunomiya University, Mine, Utsunomiya, 321-8505, Japan*

(Dated: June 16, 2023)

We present a novel method, IMSRG-Net, which utilizes machine learning techniques as a solver for the in-medium Similarity Renormalization Group (IMSRG). The primary objective of IMSRG-Net is to approximate the Magnus operators $\Omega(s)$ in the IMSRG flow equation, thereby offering an alternative to the computationally intensive part of IMSRG calculations. The key idea of IMSRG-Net is its design of the loss function inspired by physics-informed neural networks to encode the underlying *physics*, i.e., IMSRG flow equation, into the model. Through training on a dataset comprising ten data points with flow parameters up to $s = 20$, capturing approximately one-eighth to one-quarter of the entire flow, IMSRG-Net exhibits remarkable accuracy in extrapolating the ground state energies and charge radii of ^{16}O and ^{40}Ca . Furthermore, this model demonstrates effectiveness in deriving effective interactions for a valence space.

Introduction. The in-medium Similarity Renormalization Group (IMSRG) method [1–5] is a highly powerful framework to study nuclear many-body systems. This method serves as an *ab initio* technique for investigating the properties of nuclei near sub-shell closures, while also enabling the systematic derivation of effective interactions and operators for a valence space. The IMSRG method is formulated by the unitary transformation of operators, such as the Hamiltonian, through the IMSRG flow equation. The objective is to decouple a target subspace from the rest of many-body Hilbert space. For ground state calculations, this entails decoupling particle-hole excitations from the reference state, whereas for deriving effective interactions, the focus is on decoupling the valence space from the core and outside (excluded) space. Notably, recent studies have extended the application of the IMSRG to heavier nuclei, such as ^{132}Sn and ^{208}Pb [6, 7].

Although the IMSRG method is a powerful approach, it is still computationally demanding to perform numerous calculations for different nuclei and input nuclear interactions. Consequently, it is crucial to develop efficient methods for conducting IMSRG calculations. The construction of such emulators or surrogate models has emerged as a prominent research topic within the nuclear physics community, providing as a key tool for comprehending and evaluating the uncertainties associated with nuclear many-body calculations and realistic nuclear potentials. A notable example of such emulators is the eigenvector continuation (EC) method [8–10], which has been extensively applied to diverse nuclear many-body problems [11–20]. Its significance has been recognized from a broader perspective as model order reduction [21]. However, applying the EC method to IMSRG calculations poses challenges since the EC method primarily operates on many-body wave functions (eigenvectors of a Hamiltonian), while IMSRG calculations are performed on many-body operators, such as the Hamiltonian.

In this work, we present an alternative approach to constructing a surrogate model for IMSRG, employing a data-driven technique based on machine learning. The nuclear physics

community has witnessed diverse applications of machine learning-based models to replicate or assist nuclear many-body calculations (see, e.g., Refs. [22]). We propose a machine-learning-based solver for the IMSRG flow equation, named IMSRG-Net, which is inspired by the physics-informed neural network (PINN) [23, 24]. The primary objective of this study is to provide a proof of concept, exploring the potential of data-driven approaches in constructing surrogate models for IMSRG methods, rather than aiming to accelerate the cutting-edge IMSRG calculations on supercomputers. The test grounds for the proposed method are IMSRG calculations of ground state energies and charge radii of ^{16}O and ^{40}Ca , and derivation of effective interactions for *sd*- and *pf*-shell nuclei.

Methodology. Here, we briefly review the basics of in-medium similarity renormalization group (IMSRG) method. In IMSRG methods, one starts from a normal-ordered Hamiltonian $H(s = 0)$ on a reference state, and then performs the unitary transformation $U(s)$ to decouple particle-hole excitations from the reference state

$$H(s) = U(s)H(0)U^\dagger(s), \quad (1)$$

where s is the flow parameter. This gives the following IMSRG-flow equation:

$$\frac{dH(s)}{ds} = [\eta(s), H(s)], \quad (2)$$

$$\eta(s) \equiv \frac{dU(s)}{ds}U^\dagger(s) = -\eta^\dagger(s). \quad (3)$$

In the last decade, significant progress has been made in solving the IMSRG flow equation employing the Magnus expansion [25]. Within the Magnus formulation of the IMSRG, the unitary transformation in Eq. (1) is explicitly evaluated by

$$U(s) = e^{\Omega(s)}, \quad (4)$$

$$\frac{d\Omega(s)}{ds} = \eta(s), \quad (5)$$

with the anti-Hermitian Magnus operator $\Omega(s)$. The second equation follows from Eq. (3). By doing this, one can write down the transformations of any operators $O(s)$ including the

* syoshida@cc.utsunomiya-u.ac.jp

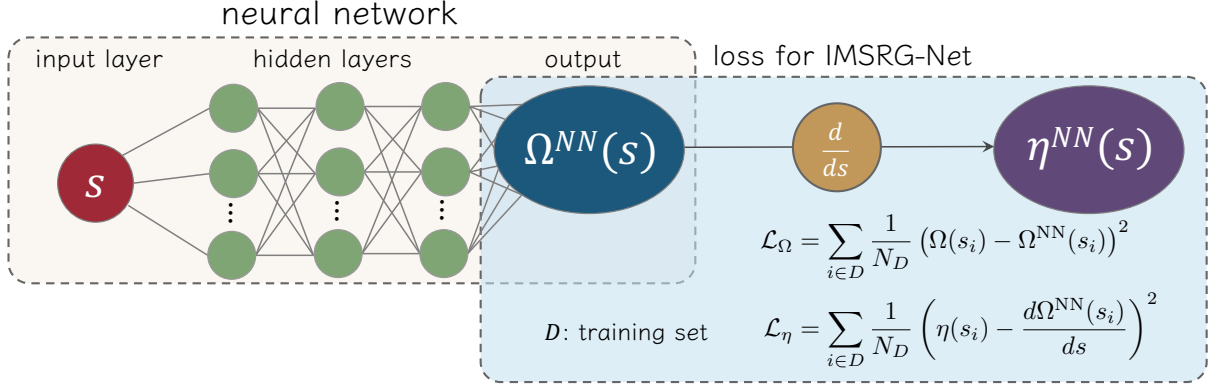


FIG. 1. Schematic of IMSRG-Net. A fully connected neural network is used to generate approximated Magnus operators $\Omega^{NN}(s)$ and their derivatives $\eta^{NN}(s)$ are used as indicators of how well a neural network model respects the underlying IMSRG flow equation. Both the loss terms on Ω and η are back-propagated to train the network.

Hamiltonian $H(s)$ as

$$O(s) = e^{\Omega(s)} O(0) e^{-\Omega(s)}. \quad (6)$$

The flow equation Eq. (2) is now translated into the ordinary differential equation for $\Omega(s)$ and the *adjoint* of $\eta(s)$

$$\frac{d\Omega}{ds} = \sum_{k=0}^{\infty} \frac{B_k}{k!} ad_{\Omega}^{(k)}(\eta), \quad (7)$$

$$ad_{\Omega}^{(k)}(\eta) = \left[\Omega, ad_{\Omega}^{(k-1)}(\eta) \right], \quad (8)$$

$$ad_{\Omega}^{(0)}(\eta) = \eta, \quad (9)$$

where we omit the explicit dependence of Ω and η on the flow parameter s , and B_k is the Bernoulli number. One can evaluate evolved operators, Eq. (6), through the Baker-Campbell-Hausdorff (BCH) formula.

Throughout this work, we employ the so-called IMSRG(2) truncation, where all operators are truncated up to the normal-ordered two-body (NO2B) level. We restrict ourselves to consider the IMSRG with a single spherical reference state and to use the so-called arctangent generator for $\eta(s)$. The interested readers are referred to Refs. [4, 5, 26] for additional information on extensions of the IMSRG method, such as different basis states, generator choices, higher order contributions, and more.

In any solvers, the IMSRG flow is discretized using a small finite step size, which in our case is set to $ds = 0.25$. As a practical measure, one additionally splits IMSRG flows into multi-steps by monitoring the norms of $\Omega(s)$ to prevent divergence and large computational time for evaluating deeply nested commutators. To simplify the discussions, however, we do not employ such a multi-step partitioning of the Magnus operators in this work other than a partitioning when turning to a valence space decoupling.

IMSRG-Net. We describe the design of the neural network architecture and the training strategy for the proposed model, IMSRG-Net. As shown in Fig. 1, the network architecture of IMSRG-Net is simple. The whole layers are the so-called fully

connected layers (also referred to as Affine layers), which consist of the input layer, three hidden layers, and the output layer. The network is regarded as a function to give an approximation of the Magnus operators, $\Omega^{NN}(s)$, for larger values of s region giving converged results. The objective of the network is to predict not observables, but the Magnus operators. Hence, once the network is trained to predict $\Omega(s)$ accurately, it is guaranteed that the network reproduces the IMSRG results for any observables.

The number of hidden layers is three, and the number of nodes for each hidden layer is 48, 48, and 16 from the input side to the output side, respectively. The adopted activation functions are the hyperbolic tangent for the first hidden layer and the softplus [27] for the remaining hidden layers.

The weights and bias parameters of the network is trained through the following loss functions on Ω^{NN} and its derivative $\eta^{NN} \equiv d\Omega^{NN}/ds$, where the superscript NN represents the values obtained through the neural network model. The loss function is the sum of the mean-squared errors (MSEs) for Ω^{NN} and η^{NN} :

$$\mathcal{L} = \mathcal{L}_\Omega + \lambda_\eta \mathcal{L}_\eta, \quad (10)$$

$$\mathcal{L}_\Omega = \sum_{i \in D} \frac{1}{N_D} (\Omega(s_i) - \Omega^{NN}(s_i))^2, \quad (11)$$

$$\mathcal{L}_\eta = \sum_{i \in D} \frac{1}{N_D} \left(\eta(s_i) - \frac{d\Omega^{NN}(s_i)}{ds} \right)^2, \quad (12)$$

where D is the training data set and N_D is the number of data. The parameter λ_η is introduced to balance the two terms. The typical size of \mathcal{L}_η can be different from that of \mathcal{L}_Ω . From our investigations, a rule of thumb to make training stable is to set $\lambda_\eta = 10^1 \sim 10^3$, which makes the contribution of Eq. (12) comparable to Eq. (11). We use a fixed value, $\lambda_\eta = 10^2$, throughout this work. The derivatives $d\Omega^{NN}/ds$ can be evaluated by automatic differentiation or numerical differentiation. We used the latter method, which is faster than the former one in our model having a large number of nodes in the output layer. IMSRG-Net can be considered as a special case of physics-informed neural networks (PINNs) [23,

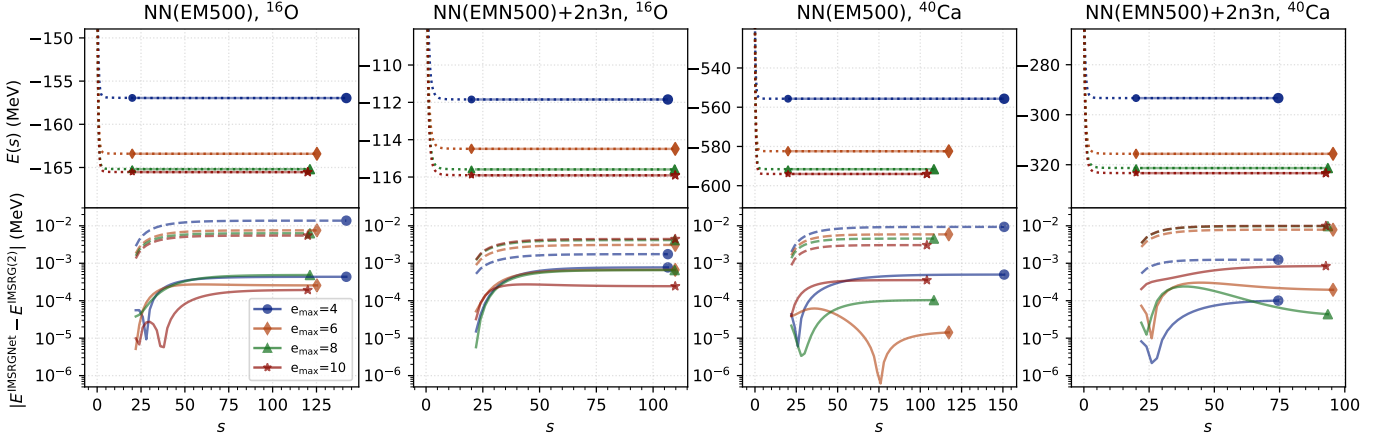


FIG. 2. Ground state energies of ^{16}O and ^{40}Ca obtained using IMSRG(2) and IMSRG-Net. In the upper panels, the dashed lines correspond to the results of IMSRG(2), while the solid lines are the results of IMSRG-Net (for $s > 20.0$). The markers are placed on the right edge of the lines to represent the points where IMSRG(2) calculations converged. The lower panels illustrate the energy differences between IMSRG(2) and IMSRG-Net. The solid lines represent the results of IMSRG-Net with $\lambda_\eta = 10^2$, and the dashed ones represent results with $\lambda_\eta = 0$. Further information regarding the input potentials, NN(EM500) and NN(EMN500)+2n3n, can be found in the main text.

24]. Each component of η contains information regarding the channels to be decoupled. Such physics information is encoded through the \mathcal{L}_η term, serving as a soft constraint that guides the network to learn the underlying principle – the IMSRG flow equation.

We employed the AdamW optimizer [28] to train the network, updating the model parameters through the back-propagation based on the loss function Eq. (10). Empirically, we observed that the model exhibits superior extrapolation performance when using AdamW compared to the Adam optimizer [29] with the same hyperparameters. This may originate from the fact that the weight decay term in AdamW prevents the overfitting. To accelerate the learning process and mitigate the overfitting, we adopted mini-batch learning. The hyperparameters, including network architecture, optimizers, their parameters, activation functions, etc., are kept fixed throughout the study. Further technical details regarding our hyperparameter exploration can be found in the Supplemental Material [30].

The operators of interests, Ω and η , are vectorized and divided into the three distinct data sets: 10 training data $\{s = 17.75, 18.0, \dots, 20.0\}$, 5 validation data $\{s = 16.5, \dots, 17.5\}$, and test data $\{s = \infty\}$. Here, $s = \infty$ corresponds to the point at which IMSRG(2) converged, with $\|\eta(s)\| < \epsilon_{\text{norm}}$ as the convergence criterion $\sim 10^{-6}$, which is one employed in IMSRG codes [31, 32]. The training set is used to train the network, while the test data is used to assess the accuracy of the extrapolation by the model. Using the validation data, we select the model that minimizes the sum of the training loss Eq. (10) and MSE of the validation set across all epochs as the best model. The number of training data points was determined by compromise between the number of data and the memory cost. As expected, using data points closer to $s = \infty$ naturally leads to higher accuracy and vice versa. However, in this study, the maximum value of s used as training data was set to 20. This value typically corresponds to the first 1/8 to 1/4 of the entire IMSRG flow. In this case, the results are not

significantly affected by a particular number of data points as long as the number of training data exceeds ~ 5 .

In our numerical calculations, all Ω values are defined as residuals relative to a reference value $\Omega(s_t)$ such that s_t represents the largest value in the training set, which is $s_t = 20.0$ in the present study. This works as a normalization between different problems and justifies the consideration of multiple tasks using the same architecture. Additionally, the residuals of the Ω are multiplied by a global scaling factor. Normalizing high-dimensional vectors solely by the standard deviation of the data can sometimes lead to overflow issues. To address this, we have determined that the scaling factor, chosen as $\min\{1/\text{std}(\Omega), 10^3\}$, is suitable for the current model and target nuclei. It is important to note that the optimal scaling factor may vary depending on the specific problem, and an inappropriate choice can result in both overflow and underflow during calculations.

The computational cost of IMSRG-Net is primarily determined by the size of the output layer, which depends on the size of model space specified by e_{max} truncation. While it is desirable to use GPU accelerators for training neural network models, the VRAM usage often exceeds the capacity of standard GPGPUs for larger $e_{\text{max}} > 10$. Consequently, we limit our presented results to smaller e_{max} values: 4, 6, 8, and 10. The training time for $e_{\text{max}} = 10$, involving 5,000 epochs and $ds = 0.25$ amounts to about 2.5 hours on a single NVIDIA RTX A4000 GPU. We used NuclearToolkit.jl [32] for performing IMSRG calculations, and PyTorch [33] for constructing and training the neural network model. One can reproduce the results with the codes and data on the author's GitHub repository [34].

Results. In Fig. 2, we show the results of IMSRG-Net for ^{16}O and ^{40}Ca using two different input interactions. The first interaction, denoted as EM500, consists of the so-called EM nucleon-nucleon (NN) interaction [35] regularized by a cut-off 500 MeV and softened by the similarity renormalization

TABLE I. The ground state energies and charge radii of ^{16}O and ^{40}Ca by IMSRG(2) and IMSRG-Net. The $s = \infty$ corresponds to the one giving converged value of IMSRG(2).

target	interaction	e_{max}	Energy (MeV)				R_{ch} (fm)			
			$s = 20$		$s = \infty$		$s = 20$		$s = \infty$	
			IMSRG(2)	IMSRG-Net	IMSRG(2)	IMSRG-Net	IMSRG(2)	IMSRG-Net	IMSRG(2)	IMSRG-Net
^{16}O	EM500	4	-156.9474	-156.9474	-156.9611	-156.9607	2.2578	2.2578	2.2612	2.2610
		6	-163.4079	-163.4079	-163.4153	-163.4150	2.2526	2.2526	2.2547	2.2546
		8	-165.1876	-165.1875	-165.1932	-165.1927	2.2482	2.2482	2.2499	2.2497
		10	-165.5309	-165.5309	-165.5359	-165.5357	2.2469	2.2469	2.2485	2.2484
	EMN500+2n3n	4	-111.8453	-111.8453	-111.8470	-111.8462	2.3600	2.3600	2.3607	2.3605
		6	-114.4895	-114.4895	-114.4925	-114.4918	2.3681	2.3681	2.3692	2.3690
		8	-115.5894	-115.5894	-115.5930	-115.5924	2.3735	2.3735	2.3748	2.3746
		10	-115.9040	-115.9040	-115.9079	-115.9082	2.3751	2.3751	2.3765	2.3765
^{40}Ca	EM500	4	-555.6791	-555.6791	-555.6884	-555.6879	2.5947	2.5947	2.5959	2.5958
		6	-582.4293	-582.4293	-582.4350	-582.4351	2.5960	2.5960	2.5967	2.5967
		8	-591.5783	-591.5782	-591.5822	-591.5821	2.5915	2.5915	2.5920	2.5920
		10	-594.0215	-594.0215	-594.0242	-594.0246	2.5890	2.5890	2.5894	2.5895
	EMN500+2n3n	4	-293.3474	-293.3474	-293.3486	-293.3487	2.8579	2.8579	2.8581	2.8581
		6	-315.6334	-315.6334	-315.6411	-315.6409	2.9082	2.9082	2.9089	2.9088
		8	-321.3233	-321.3232	-321.3320	-321.3319	2.9201	2.9200	2.9209	2.9208
		10	-323.3519	-321.3520	-323.3605	-323.3613	2.9252	2.9252	2.9260	2.9260

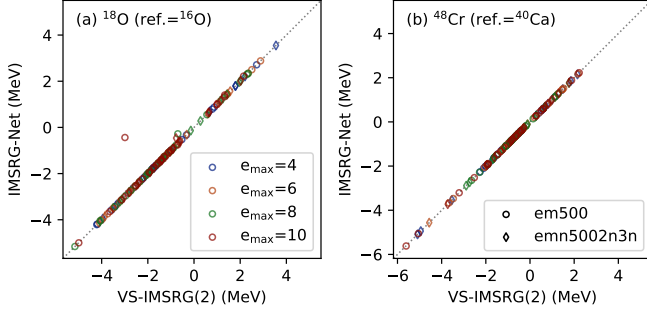


FIG. 3. Correlation plot of effective interactions derived by VS-IMSRG(2) and IMSRG-Net, (a) ^{16}O and (b) ^{48}Cr . This includes both single particle energies and two-body matrix elements, and some are randomly omitted since the number of parameters are too large to plot them all. The circle and diamond symbols represent the results of EM500 and EMN500+2n3n, respectively.

group (SRG) with $\lambda = 2.0 \text{ fm}^{-1}$. The other one, denoted as EMN500+2n3n, comprises the SRG evolved EMN interaction [36, 37] up to N4LO. The "2n3n" is representing that a density-dependent three-nucleon force [38, 39] is added to the softened EMN500 interaction. Each different symbol corresponds to results with different model spaces, specified by the e_{max} .

The upper panels in Fig. 2 display the results obtained by IMSRG(2) (dashed lines) and IMSRG-Net (solid lines for $s > 20.0$) for different e_{max} truncations. Since it is difficult to discern the differences between the two models in this scale, we show the energy differences between IMSRG(2) and IMSRG-Net in the lower panels. The solid lines in the lower panels are the results of IMSRG-Net, and the dashed ones represents cases where $\lambda_\eta = 0$. It is evident that incorporating the loss term on η is crucial for training the network and achieving

better extrapolation in the larger s region. The extrapolations exhibit an accuracy of less than 1 keV.

Table I summarizes the ground state energies and charge radii of ^{16}O and ^{40}Ca evaluated by IMSRG(2) and IMSRG-Net. The digits that differ between IMSRG(2) and IMSRG-Net are highlighted in bold. Since we extrapolated not the energies but the Magnus operators Ω to achieve unitary transformations, Eqs. (4-6), we can compute the charge radii in a straightforward manner. From the Table I, it is apparent that the results of IMSRG-Net are in good agreement with those of IMSRG(2). In both cases, energies and charge radii, one can see that the deviation between IMSRG(2) and IMSRG-Net are much smaller than the residuals which are to be obtained through the rest IMSRG flow from $s = 20$ to $s = \infty$. This level of accuracy is considered sufficient to replace the remaining flow for $s > 20$ with the proposed model.

As a natural expectation, one may consider applications of IMSRG-Net to valence-space IMSRG (VS-IMSRG) for deriving valence space effective interactions and operators. To this end, let us consider the VS-IMSRG utilizing IMSRG-Net with the same architecture above. The dataset is constructed simultaneously as the IMSRG case, utilizing $\Omega(s)$ up to $s = 20$ as the training and validation set. Note that the $s = \infty$ point for IMSRG(2) now serves as the starting point for the VS-IMSRG flow, i.e. $s = 0$.

Fig. 3 illustrates the correlation plot between the effective interactions derived by VS-IMSRG(2) and IMSRG-Net. These are effective interactions on the sd - and pf -shell model spaces employing the same input interactions as mentioned above. The reference states are chosen as the nearest doubly magic nuclei ^{16}O and ^{40}Ca . As a whole, the deviation is small, which is typically less than 1.0×10^{-8} in mean squared error, with a few exceptions for $e_{\text{max}} \geq 8$ corresponding the symbols far from the diagonal lines in Fig. 3. These exceptions correspond to the two-body matrix elements relevant to higher orbits in

the valence space, $0d_{3/2}$ for the sd shell and $0f_{5/2}$ for the pf shell. It is found that the calculation of the commutator in the BCH formula exhibits non-convergent behavior during the VS-IMSRG flow for these cases. For this reason, the failure in some components is attributed to not IMSRG-Net, but the numerical instability in VS-IMSRG.

Summary. This study explores the possibility of employing a machine-learning-based model as an alternative solver for in-medium similarity renormalization group (IMSRG). Through the utilization of the proposed neural network, IMSRG-Net, inspired by Physics-Informed Neural Networks (PINNs), we achieved extrapolation with a satisfactory level of accuracy. Energy extrapolation was accomplished with an accuracy of less than 1 keV, and the charge radii are also well reproduced with small errors of approximately 0.0001 fm. Once accurate approximations of the Magnus operators $\Omega(s)$ are obtained, any desired operators of interest can be evolved accurately using the Magnus formulation of IMSRG. This work may herald a new paradigm for the IMSRG method and offer numerous possibilities for applying PINNs-like techniques to other nuclear many-body machinery.

While we have empirically investigated the effectiveness of IMSRG-Net on various datasets, it is important to acknowledge that there may always be exceptions and cases where this network architecture or learning strategy may encounter limitations. One example is numerical instability in IMSRG itself

as shown in the valence space results. It should be noted that the numbers (energies, charge radii, and effective interactions) presented in this work are based on a single run, specifying a random seed. To reproduce the results, one can refer to the provided repository on GitHub [34], which contains the necessary information and code. The results may vary in different environments and with different random seeds, they can either be better or worse than the values reported here.

To further accelerate research workflows in the community that utilize IMSRG methods, it is desired to explore various extensions of the proposed method. For further enhancement of the accuracy of extrapolated results and improve the robustness to different target interactions and nuclei, additional inductive biases may need to be introduced. It is also crucial to develop more computationally efficient versions of IMSRG-Net. Since the current IMSRG-Net directly employs $\Omega(s)$ with large dimensions as the output layer of the neural network, it becomes challenging to store and manipulate all of them on GPGPU for cases with e_{\max} larger than 10. This limitation prevents the application of IMSRG-Net for cutting-edge IMSRG methods to larger e_{\max} cases. For instance, constructing more compact or low-rank expressions of operators while retaining as much information as possible through e.g. tensor decomposition could prove valuable.

Acknowledgments. This work was supported by JSPS KAKENHI (Grants No. 22K14030).

-
- [1] K. Tsukiyama, S. K. Bogner, and A. Schwenk, *Phys. Rev. Lett.* **106**, 222502 (2011).
 - [2] K. Tsukiyama, S. K. Bogner, and A. Schwenk, *Phys. Rev. C* **85**, 061304 (2012).
 - [3] H. Hergert, S. Bogner, T. Morris, A. Schwenk, and K. Tsukiyama, *Physics Reports* **621**, 165 (2016), memorial Volume in Honor of Gerald E. Brown.
 - [4] S. R. Stroberg, H. Hergert, S. K. Bogner, and J. D. Holt, *Annual Review of Nuclear and Particle Science* **69**, 307 (2019).
 - [5] H. Hergert, *Frontiers in Physics* **8** (2020), 10.3389/fphy.2020.00379.
 - [6] T. Miyagi, S. R. Stroberg, P. Navrátil, K. Hebeler, and J. D. Holt, *Phys. Rev. C* **105**, 014302 (2022).
 - [7] B. Hu, W. Jiang, T. Miyagi, Z. Sun, A. Ekström, C. Forssén, G. Hagen, J. D. Holt, T. Papenbrock, S. R. Stroberg, and I. Vernon, *Nature Physics* **18**, 1196 (2022).
 - [8] D. Frame, R. He, I. Ipsen, D. Lee, D. Lee, and E. Rrapaj, *Phys. Rev. Lett.* **121**, 032501 (2018).
 - [9] A. Sarkar and D. Lee, *Phys. Rev. Lett.* **126**, 032501 (2021).
 - [10] A. Sarkar and D. Lee, *Phys. Rev. Res.* **4**, 023214 (2022).
 - [11] S. König, A. Ekström, K. Hebeler, D. Lee, and A. Schwenk, *Physics Letters B* **810**, 135814 (2020).
 - [12] P. Demol, T. Duguet, A. Ekström, M. Frosini, K. Hebeler, S. König, D. Lee, A. Schwenk, V. Somà, and A. Tichai, *Phys. Rev. C* **101**, 041302 (2020).
 - [13] P. Demol, M. Frosini, A. Tichai, V. Somà, and T. Duguet, *Annals of Physics* **424**, 168358 (2021).
 - [14] R. Furnstahl, A. Garcia, P. Millican, and X. Zhang, *Physics Letters B* **809**, 135719 (2020).
 - [15] J. Melendez, C. Drischler, A. Garcia, R. Furnstahl, and X. Zhang, *Physics Letters B* **821**, 136608 (2021).
 - [16] C. Drischler, M. Quinonez, P. Giuliani, A. Lovell, and F. Nunes, *Physics Letters B* **823**, 136777 (2021).
 - [17] S. Wesolowski, I. Svensson, A. Ekström, C. Forssén, R. J. Furnstahl, J. A. Melendez, and D. R. Phillips, *Phys. Rev. C* **104**, 064001 (2021).
 - [18] D. Bai and Z. Ren, *Phys. Rev. C* **103**, 014612 (2021).
 - [19] M. Companys Franzke, A. Tichai, K. Hebeler, and A. Schwenk, *Physics Letters B* **830**, 137101 (2022).
 - [20] S. Yoshida and N. Shimizu, *Progress of Theoretical and Experimental Physics* **2022** (2022), 10.1093/ptep/ptac057, 053D02.
 - [21] J. A. Melendez, C. Drischler, R. J. Furnstahl, A. J. Garcia, and X. Zhang, *Journal of Physics G: Nuclear and Particle Physics* **49**, 102001 (2022).
 - [22] A. Boehnlein, M. Diefenthaler, N. Sato, M. Schram, V. Ziegler, C. Fanelli, M. Hjorth-Jensen, T. Horn, M. P. Kuchera, D. Lee, W. Nazarewicz, P. Ostroumov, K. Orginos, A. Poon, X.-N. Wang, A. Scheinker, M. S. Smith, and L.-G. Pang, *Rev. Mod. Phys.* **94**, 031003 (2022).
 - [23] M. Raissi, P. Perdikaris, and G. Karniadakis, *Journal of Computational Physics* **378**, 686 (2019).
 - [24] G. E. Karniadakis, I. G. Kevrekidis, L. Lu, P. Perdikaris, S. Wang, and L. Yang, *Nature Reviews Physics* **3**, 422 (2021).
 - [25] T. D. Morris, N. M. Parzuchowski, and S. K. Bogner, *Phys. Rev. C* **92**, 034331 (2015).
 - [26] M. Heinz, A. Tichai, J. Hoppe, K. Hebeler, and A. Schwenk, *Phys. Rev. C* **103**, 044318 (2021).
 - [27] H. Zheng, Z. Yang, W. Liu, J. Liang, and Y. Li, in *2015 International Joint Conference on Neural Networks (IJCNN)* (2015) pp. 1–4.
 - [28] I. Loshchilov and F. Hutter, “Decoupled weight decay regularization,” (2019), [arXiv:1711.05101 \[cs.LG\]](https://arxiv.org/abs/1711.05101).

- [29] D. P. Kingma and J. Ba, in *3rd International Conference on Learning Representations, ICLR 2015, San Diego, CA, USA, May 7-9, 2015, Conference Track Proceedings*, edited by Y. Bengio and Y. LeCun (2015).
- [30] S. Yoshida, “Supplementary material. the url will be inserted by the publisher.” ().
- [31] S. R. Stroberg, <https://github.com/ragnarstroberg/imsrg>.
- [32] S. Yoshida, *Journal of Open Source Software* **7**, 4694 (2022); NuclearToolkit.jl, <https://github.com/SotaYoshida/NuclearToolkit.jl>.
- [33] A. Paszke, S. Gross, F. Massa, A. Lerer, J. Bradbury, G. Chanan, T. Killeen, Z. Lin, N. Gimelshein, L. Antiga, A. Desmaison, A. Kopf, E. Yang, Z. DeVito, M. Raison, A. Tejani, S. Chilamkurthy, B. Steiner, L. Fang, J. Bai, and S. Chintala, in *Advances in Neural Information Processing Systems 32* (Curran Associates, Inc., 2019) pp. 8024–8035.
- [34] S. Yoshida, <https://github.com/SotaYoshida/IMSRGNet>.
- [35] D. R. Entem and R. Machleidt, *Phys. Rev. C* **68**, 041001 (2003).
- [36] D. R. Entem, N. Kaiser, R. Machleidt, and Y. Nosyk, *Phys. Rev. C* **91**, 014002 (2015).
- [37] D. R. Entem, R. Machleidt, and Y. Nosyk, *Phys. Rev. C* **96**, 024004 (2017).
- [38] M. Kohno, *Phys. Rev. C* **88**, 064005 (2013); *Phys. Rev. C* **96**, 059903 (2017).
- [39] S. Yoshida, “Exploring medium mass nuclei using effective chiral nucleon-nucleon interactions,” (2022), [arXiv:2208.02464](https://arxiv.org/abs/2208.02464) [nucl-th].

Supplemental Material

In this supplemental material, we provide technical details involved in constructing and training the proposed neural network model, IMSRG-Net.

Survey on the neural network hyperparameters

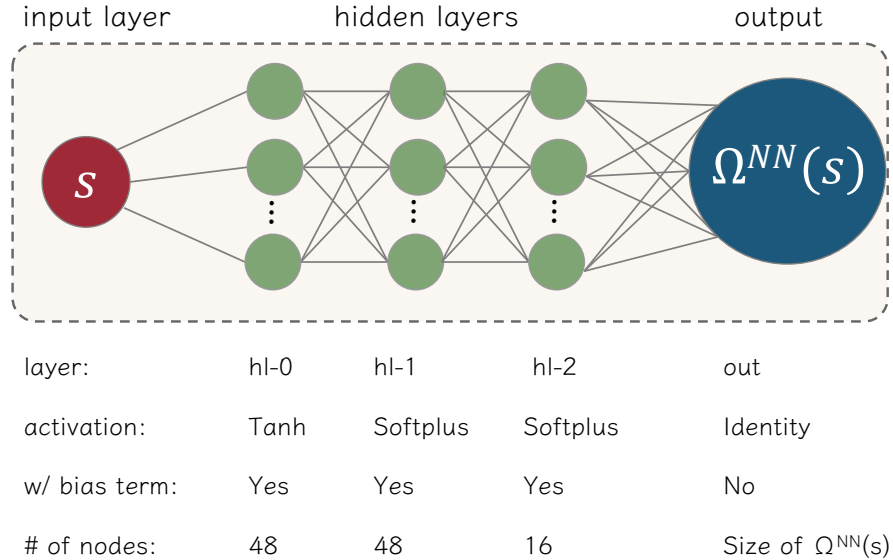


FIG. 4. Detailed design of IMSRG-Net.

The detailed architecture of IMSRG-Net is presented in Fig. 4. We have explored various combinations of hyperparameters for neural network models:

- Optimizers: stochastic gradient descent (SGD), Adam, AdamW, L-BFGS
- Activation functions: Tanh, softplus, ReLU, LeakyLU, ELU
- Number of hidden layers: 1,2,3,4
- Number of nodes in hidden layers: 4,8,16,32,48,64
- Parameters for optimizers (learning rate, weight decay, momentum, etc.)

Naturally, these trials do not cover all possible combinations of hyperparameters. Thus, it is important to remark that the architecture and hyperparameters adopted in the main text represent only one of the viable choices that can achieve the desired accuracy for the target problems.

Regarding activation functions, one of the popular choices today is the rectified linear unit (ReLU), particularly in deep neural network models for e.g. image recognition tasks, due to its computational efficiency and ability to mitigate the vanishing gradient problem. However, in our case, we found that smooth activation functions perform better than ReLU. This may be attributed to the fact that $\Omega(s)$ is a smooth function of s . For this reason, we employed the hyperbolic tangent (Tanh) function for the first hidden layer. The Softplus function, employed in the other hidden layers, achieves both smooth outputs and avoiding the vanishing gradient problem.

As explained in the main text, we utilized AdamW as the optimizer for training the model. AdamW efficiently finds (local) minima and outperforms over the other methods listed above in terms of the test accuracy and efficiency. The superiority of AdamW over the commonly used Adam optimizer may be attributed to its inclusion of a weight decay term, which penalizes large values of weight parameters and thereby mitigate the overfitting.

During each epoch, we did not use the entire dataset at once, but rather used a subset of the training data. This approach, known as mini-batch learning, is a common technique to accelerate the learning process and prevent overfitting. Specifically, we set the batch size equal to the number of data points, which is also referred to as online learning. By combining weight decay in AdamW and mini-batch learning (online learning), we achieved extrapolation without sacrificing generalization ability.

The number of nodes in the hidden layers is fixed to 48 for upstream layers (hl-0 and hl-1 in Fig. 4) and 16 for the downstream layer (hl-2). While the former one is almost irrelevant to the generalization ability of our model, we found that a larger value around 48 speeds up the training process. On the other hand, the number of nodes in the last hidden layer closest to the output layer significantly influences both accuracy and computational cost. Generally, a larger value yields better accuracy on the training, validation, and test sets, but a smaller value is preferable in terms of computational efficiency. We found that the value of 16 is a good compromise between accuracy and VRAM usage.

In IMSRG-Net, operators are stored in the form of a vector:

$$\Omega(s) = (\Omega^{(0)}, \Omega_{ij}^{(1)}, \dots, \Omega_{ijkl}^{(2)}, \dots), \quad (13)$$

where the superscripts denote the zero-, one-, two-body parts of the operator, respectively. The dimension of the vector is primarily determined by the number of elements in the two-body part $\{\Omega_{ijkl}^{(2)}\}$. Table II shows the sizes of tensors as a function of e_{\max} . To construct fully connected neural network, these numbers are multiplied by the number of nodes in the hidden layer closest to the output layer, which governs the size of the weight parameters. In addition to storing those weight parameters, the VRAM is also used to store computational graphs, gradients, and other temporary variables. Despite the total size of the tensors is depending on the choice of optimizers, VRAM usage easily exceeds 20 GB for e_{\max} larger than 10.

TABLE II. The number of elements and size of tensors as a function of e_{\max} .

e_{\max}	# of element	size(Float32) [MB]
4	34,334	0.1
6	467,076	1.8
8	3,526,724	13
10	18,345,624	70
12	73,842,358	282
14	246,457,592	940

Code and data availability

To construct and train IMSRG-Net, we used PyTorch [33], which is a popular deep learning framework in Python. The sample script and data are available at the author's GitHub repository [34], and results can be reproduced by combining them with the NuclearToolkit.jl [32].